HIGH PERMEABILITY PERMALLOY FOR MEMS

Michael Glickman[1], Trevor Niblock[2], Jere Harrison[1], Ira B. Goldberg[1], Peter Tseng[1], and Jack W. Judy[1]*
[1]Electrical Engineering Department, University of California, Los Angeles, CA, USA
[2]Magzor, Inc. Thousand Oaks, CA,

ABSTRACT

We have demonstrated a thick electrodeposition process for NiFe 80/20 (Permalloy80) that can achieve a permeability of 8500 as measured by VSM and *in situ* measurements. The key features of our electroplating process that have enabled us to obtain this permeability are: electroplating in an inert N_2 atmosphere, separating the anode from the cathode by means of a porous plastic frit, and agitating the wafer with an array of parallel fins less than 500 μm from the wafer surface. This electrodeposition method could be used to produce a wide variety of magnetic MEMS sensors and actuators that consume far less power.

INTRODUCTION

Magnetic MEMS have the promise to produce very powerful actuators and sensitive sensors, but have been limited by the difficulty of depositing thick high-quality magnetic material on the microscale [1, 2]. There are a wide variety of ferromagnetic alloys that can be plated for magnetic MEMS, but many materials have very high internal stress, making them difficult to use in released structures or for thick layers. These materials curl up or buckle when released, thereby deforming the engineered structures. Therefore, most magnetic MEMS processes are done with either NiFe 80/20 (80% Ni and 20% Fe) or nickel. Nickel is the simplest to plate, and can have very low stress. However, the permeability is significantly lower than that of permalloy, and it has a lower saturation magnetization.

NiFe 80/20, is popular because of its ability to be plated very thickly (> 100 μm), fairly low stress, low magnetostriction, good mechnanical properties, excellent corrosion resistance, reasonably high saturation (1 to 1.1 T), and relatively high permeability (200 to 5000) as shown in (Fig.1) [3–9]. Permalloy has been widely used in magnetic recording heads, and demonstrated for use in micropumps [10], magnetic micromotors [11], microrelays and switches [12], delta-wing control [7], magnetic separators [13], and microfluxgate magnetometers [14].

Other alloys, such as NiFeMo have demonstrated maximum relative permeabilities of up to 20,000 (corrected for demagnetization), but with 300% higher stress than NiFe 80/20, and has only successfully been electroplated to 5 μm. This work demonstrates electroplated NiFe 80/20 with a permeability of 8500 that is significantly higher than the highest previously reported NiFe 80/20 permeability of 5000. The improvement in permeability is achieved without using new additives, high temperature annealing or a magnetic field during plating (Fig. 1) [3–9]. In addition, the high permeability electrodeposit also maintains the other favorable properties of NiFe 80/20.

Plating nickel-iron alloys effectively is difficult for several reasons. The first reason is that nickel and iron must be deposited at the same time (codeposition) and at a precise ratio. In theory, this deposition rate is determined by the galvanic potential at the electrode surface and the concentration of the individual ions in the bath, but in practice, iron (the less noble metal), is deposited preferentially to nickel, which makes the codeposition anamalous [15]. To compensate for the faster iron deposition, the Ni^{2+} / Fe^{2+} ratio in the electroplating solution is made to be much higher than the desired stoichiometry of the electroplated material, so that the iron becomes mass-transfer limited. As a consequence, the concentration of iron in the deposited material is determined by the diffusion of iron ions to the working electrode. Therefore, it is important for all electroplated surfaces to be adequately and uniformly agitated, so the percent of Fe in the deposit can be controlled more easily. Variations in the composition can lead to higher coercivity and lower permeability [6].

An important concern is that during plating, Fe^{2+} is oxidized to Fe^{3+} at the surface of the anode or when exposed to oxygen and a sufficiently low pH through the reaction,

$$2Fe^{2+} + 2H^{+} + \tfrac{1}{2}O_2 \rightarrow 2Fe^{3+} + H_2O\ . \qquad (1)$$

The Fe^{3+} can then form an insoluble iron-oxide compound called hematite $FeO(OH)_{(s)}$, which can then contaminate the electroplated material. In addition Fe^{2+} reduces more readily at the working electrode (the wafer), than Fe^{3+}, which reduces the quantity of iron deposited in the film. Because the plating efficiency is not 100%, hydrogen bubbles that form at the wafer surface during plating can be incorporated into the film if the agitation is inadequate [16]. The hydrogen bubbles create voids in the film that lead to lower saturation magnetization and permeability. By addressing the aformentioned concerns, our electroplating system is able to substantially improve permeability using a typical NiFe 80/20 electroplating bath (Table 1). First we will discuss our electroplating setup, then our measurement methods.

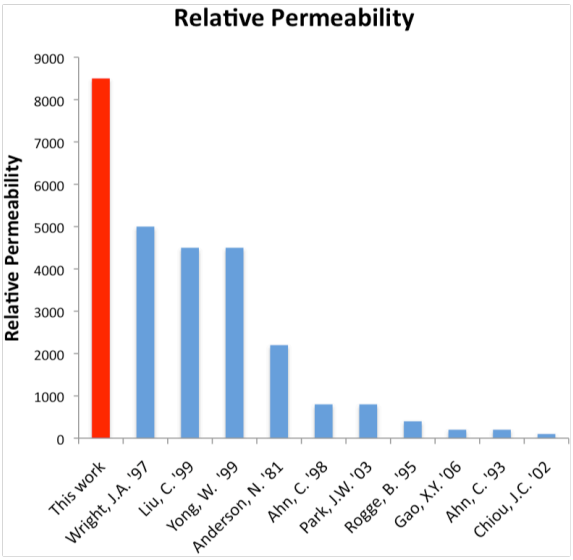

Figure 1: Comparison of maximum permeability of various published work.

Ingredient	Concentration
Nickel Sulfate Hexahydrate	250 g/l
Ferrous Sulfate Heptahydrate	5 g/l
Boric Acid	25 g/l
Sodium Saccharin	1 g/l
Sodium Lauryl Sulfate	0.1 g/l

Table 1: The plating recipe.

EXPERIMENTAL SETUP

During electroplating, the low levels of iron in the bath become depleted near the counter-electrode surface (the wafer). In order to help ensure uniform stoichiometry, the electroplating surface should be replenished with fresh solution by vigorous agitation. In addition, the uniform distribution of additives, such as saccharin and sodium lauryl sulfate, help to create more uniform material deposition and morphology. To achieve vigorous agitation, we built an agitator with multiple fin-like structures that move perpendicular to the plane of the wafer, as shown in Fig 2. The fins are less than 0.5 mm from the wafer in order to force the movement of solution across the wafer. This method of agitation uniformly agitates the solution and reduces the thickness of the diffusion boundary layer [17]. The agitator fins are moved by an external motor and rod to convert the rotational movement to linear movement. The agitator travels 11.7 cm for each rotational cycle of the motor, and is operated at 30 RPM, for a fin speed of 5.8 cm/s. The plating is current controlled at 5 mA/cm^2, and at room temperature (22^{o}C).

As the fins of the agitator repeatedly move across the wafer, they physically remove any accumulated hydrogen bubbles, which results in a smoother and denser film with higher permeability. In addition to removing hydrogen bubbles and ensuring a uniform mixture, the thinning of the boundary layer allows for more uniform height distribution of different sized openings, as shown in Fig. 3 [17].

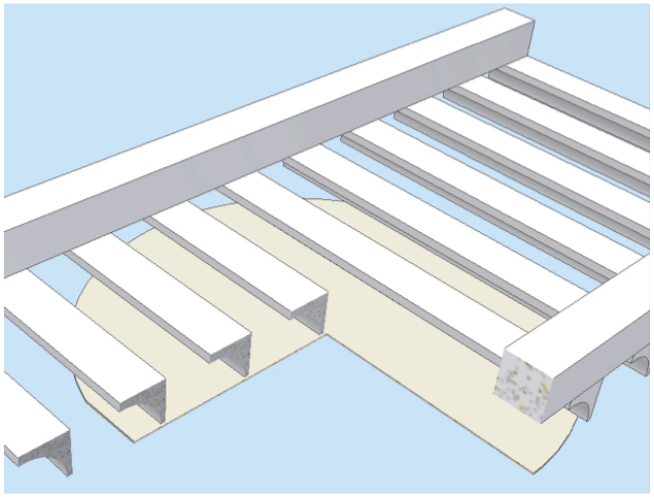

Figure 2: A 3/4 view of multi-fin agitation scheme over a wafer.

To ensure that Fe^{2+} is not oxidized to Fe^{3+} at the anode surface, one must keep the anode surface in a solution that is free of iron ions, yet maintains conductivity with the rest of the solution. The separation is accomplished by keeping the pure Ni mesh anode in a container filled with plating solution that does not contain Fe ions. The anode and its neighboring solution are separated from the cathode and its neighboring solution by a porous plastic sheet with a 10 μm pore size as shown in Fig 4. Over the relatively short timescales of electrodeposition (~ 3 hrs), Ni ions are driven by an electric-field gradient across the membrane to allow for plating, but little iron diffuses back across the membrane. In addition, the porous barrier contains most of the contaminating Ni particles that are shed during the electrochemical etching of the anode.

Because Fe^{2+} can be oxidized to Fe^{3+} by dissolved oxygen, the plating solution should not be exposed to air for extended periods of time, as this would cause particulates to form in the solution and then plate onto the wafer. To prevent particulate formation, the plating solution is always kept under nitrogen atmosphere. Additionally, the solution must be filtered using a 100-nm-pore-diamerter filter, since hematite particles have nanoscale dimensions, in the event of oxygen intrusion.

Since the filter has such diameter small pores, we use a large-surface-area (Polycap* TF Disposable Filter Capsule Whatman, Maidstone, Kent UK), which has an effective surface area of 1000 cm^2, and thus impose a minimal fluidic resistance. A low fluidic resistance is important because the plating bath is pumped by a peristaltic pump to minimize contamination of the bath. The filter is placed between the reservoir and the plating tank to prevent hematite particles that form in the reservoir from passing into the plating tank. The storage reservoir allows nitrogen to be bubbled through the solution continuously in a stoppered flask. The anode compartment is stored in a nickel-containing solution when not in use.

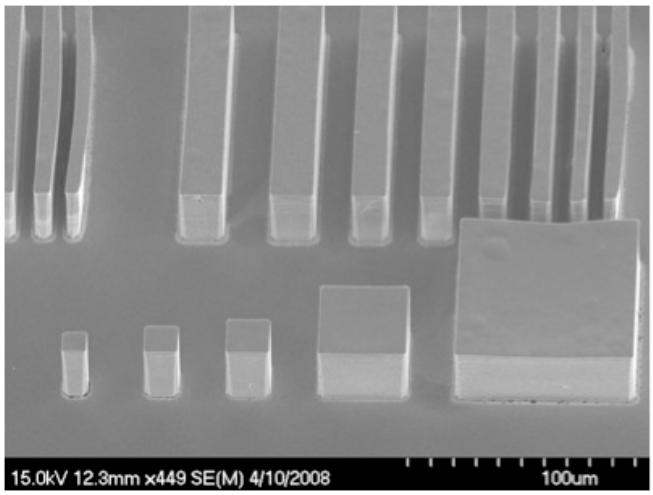

Figure 3: Permalloy deposited to 30 μm.

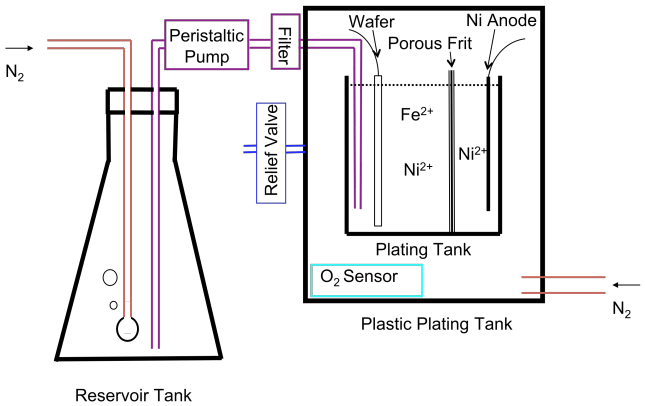

Figure 4: A schematic diagram of the NiFe 80/20 electroplating setup. The agitator and wafer chuck are not shown.

MAGNETIC PROPERTIES

The magnetic properties of the electroplated NiFe 80/20 were measured by two methods. The first method was by vibrating sample magnetometer (VSM) using 6-mm-diameter samples of 400 nm and 7 μm thickness, as measured by a surface profilometer (Veeco Dektak 6, Edina, MN, USA). When electropating samples, it is important not to cut or break the film, as this can create large coercivites on the edge of the sample, so we electroplated through a 10-μm-thick KMPR mold (a negative photoresist with vertical sidewalls). The samples were cleaved from the wafer (exterior to the electroplated region) and placed in the 7300-series VSM (Lake Shore Cryotronics, Inc., Westerville, OH, USA) to obtain an *M-H* plot (Fig. 5), from which we could calculate the apparent permeability,

$$\mu_a = (M/H) + 1 \ . \qquad (2)$$

The apparent permeabiltiy μ_a is a very strong function of the material geometry as shown in Fig. 6. The demagnetization factor D of a thin disk has been solved analytically by Chen *et al.* [18], so there is no need to use an ellipsoidal approximation. Using the calculated demagnetization factor, we must convert the apparent permeability to an actual relative material permeability μ_r using the formula

$$\mu_r = (\mu_a - \mu_a D) / (1 - \mu_a D) \ , \qquad (3)$$

which can result in substantial errors if the true permeability is of the order of $1/D$, as shown in Fig. 7. If a sample dimension with too large of a demagnetization factor is chosen, tiny errors due to VSM drift or inaccuracies in sample thickness measurement can lead to an order-of-magnitude error when the true material permeability is estimated from the apparent permeability.

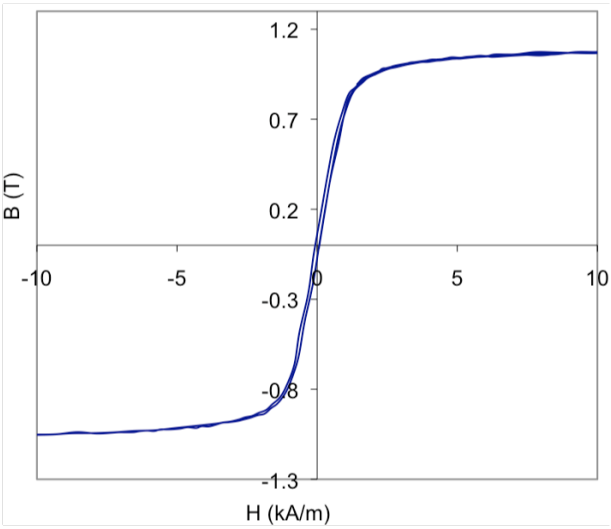

Figure 5: NiFe 80/20, not corrected for demagnetization factor.

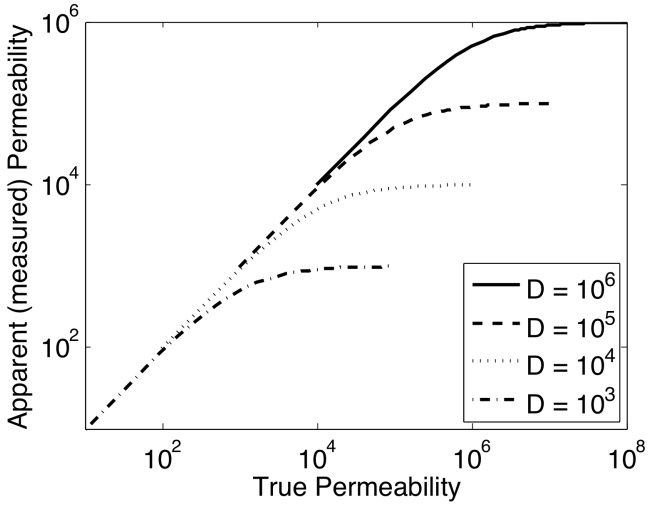

Figure 6: The apparent permeability for various demagnetization factors. The apparent permeability asymptotes to $(1/D) + 1$ *for infinite permeability.*

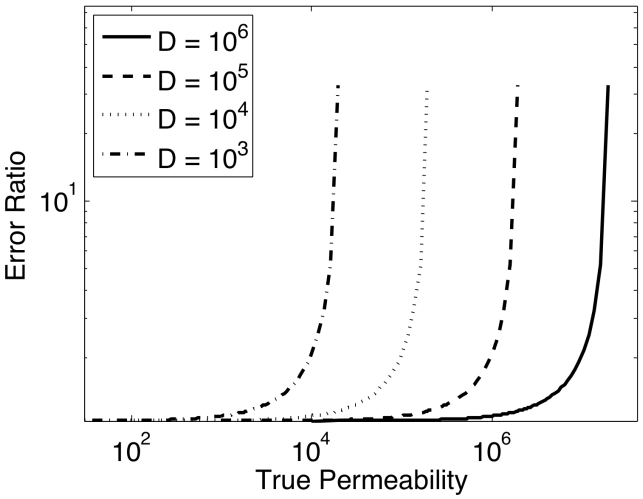

Figure 7: Ratio of calculated relative permeability to actual permeability, for a 5 % measurement error for various demagnetization factors, D. As the apparent permeability approaches $1/D + 1$*, the measurement becomes highly inaccurate.*

In addition to VSM measurements, we have also confirmed the permeability by *in situ* inductance measurements using a microfabricted inductor with 3D solenoidal coils (Fig. 8). We determined the maximum relative permeability by finding the maximum inductance as measured by an Agilent 4294A Impedance Analyzer at 620 Hz with an input of 5.3 mA. The inductor had 87 turns, a coil resistance of 37 Ω, a thickness of 7 μm, core width of 300 μm, and an inductance of 55 μH.

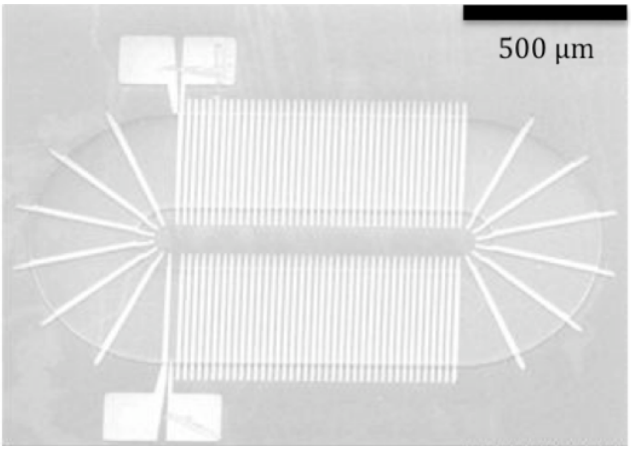

Figure 8: Inductor test structure for measuring inductance.

CONCLUSION

By using multiple knife-edge agitators to agitate the electroplating solution, we have reduced the incorporation of hydrogen bubbles into the plating bath, as well as created a more uniform composition. We have also greatly reduced hematite contamination of the electroplating solution and the conversion of Fe^{2+} to Fe^{3+}, which can affect the amount of iron deposited in the film. By combining these methods we have been able to create a film that has an order of magnitude higher permeability than a typical electrodeposited NiFe 80/20 film, and substantially higher permeability than the highest reported permeability (which gave no details on their methods).

ACKNOWLEDGEMENTS

The authors would like to thank the UCLA Nanoelectronics Research Facility for their help in the fabrication of the MEMS inductor.

REFERENCES

[1] J. Judy and N. Myung, ``Magnetic materials for MEMS," in *MRS Workshop on MEMS Materials, San Francisco, California, (April 5-6, 2002)*, pp. 23-26.

[2] N. Myung, D. Park, B. Yoo, and P. Sumodjo, ``Development of electroplated magnetic materials for MEMS," *Journal of Magnetism and Magnetic Materials*, vol. 265, no. 2, pp. 189-198, 2003.

[3] C. Ahn and M. Allen, ``Micromachined planar inductors on silicon wafers for MEMS applications," *IEEE Transactions on Industrial Electronics*, vol. 45, no. 6, pp. 866-876, 1998.

[4] X. Gao, Y. Cao, Y. Zhou, W. Ding, C. Lei, and J. Chen, ``Fabrication of solenoid-type inductor with electroplated NiFe magnetic core," *Journal of Magnetism and Magnetic Materials*, vol. 305, no. 1, pp. 207-211, 2006.

[5] J. Park and M. Allen, ``Ultralow-profile micromachined power inductors with highly laminated Ni/Fe cores: application to low-megahertz DC-DC converters," *IEEE Transactions on Magnetics*, vol. 39, no. 5, pp. 3184-3186, 2003.

[6] N. Anderson and C. Grover Jr, ``Electroplating of nickel-iron alloys for uniformity of nickel/iron ratio using a low density plating current," Jul. 21 1981, uS Patent 4,279,707.

[7] C. Liu, T. Tsao, Y. Tai, T. Leu, C. Ho, W. Tang, and D. Miu, ``Out-of-plane permalloy magnetic actuators for delta-wing control," in *Proceedings of IEEE Micro Electro Mechanical Systems (MEMS 95)*, 1995, pp. 7-12.

[8] C. Ko, J. Yang, and J. Chiou, ``Efficient magnetic microactuator with an enclosed magnetic core," *Journal of Microlithography, Microfabrication, and Microsystems*, vol. 1, p. 144, 2002.

[9] C. Liu and Y. Yi, ``Micromachined magnetic actuators using electroplated permalloy," *IEEE transactions on magnetics*, vol. 35, no. 3, pp. 1976-1985, 1999.

[10] W. Zhang and C. Ahn, ``A bi-directional magnetic micropump on a silicon wafer," in *Solid-State Sensor and Actuator Workshop, Hilton Head Island, South Carolina, June 3-6, 1996: technical digest*. The Foundation, 1996, p. 94.

[11] B. Wagner, M. Kreutzer, and W. Benecke, ``Linear and rotational magnetic micromotors fabricated using silicon technology," *IEEE Micro Electro Mechanical Systems, 1992, MEMS'92, Proceedings. An Investigation of Micro Structures, Sensors, Actuators, Machines and Robot*, pp. 183-189, 1992.

[12] M. Ruan, J. Shen, and C. Wheeler, ``Latching micro magnetic relays with multistrip permalloycantilevers," *Micro Electro Mechanical Systems, 2001. MEMS 2001. The 14th IEEE International Conference on*, pp. 224-227, 2001.

[13] T. Liakopoulos, J. Choi, and C. Ahn, ``A bio-magnetic bead separator on glass chips using semi-encapsulated spiral electromagnets," in *Solid State Sensors and Actuators, 1997. TRANSDUCERS' 97 Chicago., 1997 International Conference on*, vol. 1, 1997.

[14] T. Liakopoulos and C. Ahn, ``A micro-fluxgate magnetic sensor using micromachined planar solenoid coils," *Sensors & Actuators: A. Physical*, vol. 77, no. 1, pp. 66-72, 1999.

[15] D. Gangasingh and J. Talbot, ``Anomalous Electrodeposition of Nickel-Iron," *Journal of the Electrochemical Society*, vol. 138, p. 3605, 1991.

[16] R. Orinakova, A. Turonova, D. Kladekova, M. Galova, and R. Smith, ``Recent developments in the electrodeposition of nickel and some nickel-based alloys," *Journal of Applied Electrochemistry*, vol. 36, no. 9, pp. 957-972, 2006.

[17] B. Wu, Z. Liu, A. Keigler, and J. Harrell, ``Diffusion boundary layer studies in an industrial wafer plating cell," *Journal of the Electrochemical Society*, vol. 152, p. C272, 2005.

[18] D. Chen, E. Pardo, and A. Sanchez, ``Radial magnetometric demagnetizing factor of thin disks," *IEEE Transactions on Magnetics*, vol. 37, no. 6 Part 1, pp. 3877-3880, 2001.

CONTACT

* Michael Glickman: michael.glickman@ucla.edu